Dynamic Stall Measurements and Computations for a VR-12 Airfoil with a Variable Droop Leading Edge

P.B. Martin and K.W. McAlister
Army / NASA Rotorcraft Division
US Army Aviation and Missile Command
Aeroflightdynamics Directorate (AMRDEC)
Ames Research Center M/S 215-1
Moffett Field, CA 94035-1000

M.S.Chandrasekhara
Navy-NASA Joint Institute of Aerospace Sciences
Department of Aeronautics and Astronautics
Naval Postgraduate School
Ames Research Center M/S 260-1
Moffett Field, CA 94035-1000

W. Geissler
DLR Institute of Aerodynamics and Flow Technology
Bunsenstr 10, Goettingen D-37073, Germany

Abstract

High density-altitude operations of helicopters with advanced performance and maneuver capabilities have lead to fundamental research on active high-lift system concepts for rotor blades. The requirement for this type of system was to improve the sectional lift-to-drag ratio by alleviating dynamic stall on the retreating blade while simultaneously reducing the transonic drag rise of the advancing blade. Both measured and computational results showed that a Variable Droop Leading Edge (VDLE) airfoil is a viable concept for application to a rotor high-lift system. Results are presented for a series of 2D compressible dynamic stall wind tunnel tests with supporting CFD results for selected test cases. These measurements and computations show a dramatic decrease in the drag and pitching moment associated with severe dynamic stall when the VDLE concept is applied to the Boeing VR-12 airfoil. Test results also show an elimination of the negative pitch damping observed in the baseline moment hysteresis curves.

Introduction

Compressible dynamic stall places limits on the operational envelope of military class helicopters during maneuvers, high-speed flight, and operations at high density-altitude. These limits are a direct result of the severe unsteady forces and moments that characterize the performance of an airfoil operating through dynamic stall. A breakdown of power components describing a typical transport helicopter shows that the sea level cruise performance is primarily a function of the fuselage and hub drag ratio (see the example calculations in Fig. 1a). At moderate weights and sea level conditions, the rotor airfoils typically operate well within their range of high lift-to-drag. Recent operations in desert and mountainous regions have challenged current rotor designs with effective density-altitudes on the order of 10,000 ft. This can occur either from the requirement to operate at moderate altitudes with temperatures in excess of 100°F, or from the requirement to traverse mountainous terrain. At high density-altitude, the rotor profile power becomes equivalent to the parasite power contribution from the airframe drag at the speed for best range, V_{br} (as shown by Fig. 1). In order to increase range during missions at high density-altitude, it becomes important to improve both the airframe drag and also the rotor lift-to-drag ratio.

Two approaches for increasing the rotor lift-to-drag ratio are to decrease the transonic drag rise on the advancing blade and to decrease the stall induced drag rise on the retreating blade. One concept aimed at alleviating both of these flow physics problems is to use an active high-lift system on a portion of the rotor blades. An active high-lift system is required to simultaneously improve the lift-to-drag ratio of the airfoils on the retreating blade without compromising the advancing blade performance. Alternatively, high

Presented at the American Helicopter Society 59th Annual Forum, Phoenix, Arizona, May 6 – 8, 2003.

performance transonic airfoils could be used on the outer regions of the rotor blade. The poor high-lift performance of this type of airfoil could be overcome by the use of a drooping leading edge over the retreating side of the rotor disc.

In addition to the performance improvements, an active high-lift system might present a practical solution to common aeroelastic problems leading to excessive loads and vibration. Coupled with the elastic rotor blade motion, the onset of dynamic stall creates large unsteady pitch link loads causing vibration, rapid localized changes in blade lift and acoustic signatures, and negative torsional damping that may lead to aeroelastic instabilities. The sources of these 3D unsteady aerodynamic phenomenon occurring on full scale rotor blades are based in part on the fundamental flow physics measured in 2D oscillating airfoil wind tunnel tests. In response to emerging US Army requirements for transformation to a new generation of highly maneuverable, high speed rotorcraft, continued efforts are aimed at a better understanding of dynamic stall onset and control through experimental and numerical studies. This paper presents results from a joint US Army / DLR Goettingen cooperative dynamic stall control research program.

Compressible dynamic stall control has already been demonstrated on a symmetric NACA 0012 airfoil using the dynamically deforming leading edge (DDLE) airfoil concept (Ref. 1). In this design, the airfoil leading edge curvature was dynamically varied by as much as 320% by retracting its nose a very small (of the order of 1% chord) distance. However, the concomitant gross potential flow changes resulted in a dramatically improved airfoil instantaneous pressure distribution, which favorably influences the dynamic stall vorticity field and enables control (Ref. 1). Dynamic stall control has also been achieved using a slatted helicopter airfoil at Mach numbers of up to 0.4 (Ref. 2). In this study, different leading-edge slats were shown to be effective in preventing the formation of the dynamic stall vortex on the main element of the airfoil. The natural bleed flow through the slat-airfoil slot was sufficient to produce the desired effects. Although both the DDLE airfoil and the slatted airfoils were proven to be successful in delaying stall onset, the need to maintain a highly flexible leading edge surface in the former and the drag of the slat on the rotor advancing side with the latter approach were deemed somewhat restrictive (Ref. 3).

In an attempt to overcome these limitations, an approach known as the Variable Droop Leading Edge (VDLE) airfoil was considered (Fig. 2). A similar concept had shown promise in earlier US Army tests in a water tunnel and in incompressible flow computations (Refs. 4,5). The airfoil under consideration was a cambered airfoil with excellent performance for the advancing flow conditions. On the retreating side azimuths, a portion of the blade leading edge was drooped dynamically so that it was at a reduced incidence to the oncoming stream. Since dynamic stall is a leading edge phenomenon arising from a number of different flow mechanisms for small changes in flow conditions (Ref. 6), this approach offers a way to modify the local adverse flow effects suitably to improve the airfoil performance on the retreating side. This paper describes the approach and the early results from tests on the VDLE airfoil in the NASA Ames Fluid Mechanics Laboratory (FML) Compressible Dynamic Stall Facility (CDSF).

Description of the Experiment

The VDLE airfoil tests were conducted at Mach numbers ranging from 0.2 to 0.45 and at reduced frequencies ($k=\omega\, c/2U$) from 0 to 0.1 in the NASA Ames Research Center FML 25 cm x 35 cm CDSF. The uniqueness of the CDSF is that an airfoil is mounted between its sidewalls and is oscillated in pitch about the quarter chord as $\alpha(t) = \alpha_m - \alpha_a \sin\omega t$, where α_m is the mean angle of attack, $0^O < \alpha_m < 15^O$, and α_a is the amplitude of oscillation, $0^O < \alpha_a < 10^O$. A specially designed mechanism mounted on the top of the tunnel enables airfoil oscillation frequencies of up to 100 Hz. Ref. 7 provides a complete description of the CDSF and its instrumentation. Experimental data presented in this paper are based on optical measurements of the density field near the leading edge and 20 surface-mounted pressure transducers located on the upper and lower surfaces of the airfoil.

The Variable Droop Leading Edge Airfoil

Figure 2 shows the VDLE airfoil in two configurations: (a) the baseline VR-12 airfoil with no leading edge droop and (b) a fixed leading edge droop VR-12 airfoil. Figs. 3(a) and (b) illustrate the model assembly with the droop actuator links partially installed on the outside edges of the model. The dimensions are a 15.2 cm chord with a span of 25 cm. The complete airfoil model was built in two parts including the drooping front 25% and the fixed main element. These two sections are connected through a hinge at the intersection of the quarter-chord point with the center of the airfoil thickness.

The main element has machined rectangular tangs that are used to hold the edges in matching slots in the CDSF windows. One side of the window is shown in Fig. 3 (c) and (d). The pitch link attached to the left side of the windows oscillate the main element of the model about the quarter-chord point. The drooping portion of the airfoil is fully supported by the

hinge. The hinge axis also passes through the quarter-chord point (see Fig. 3). The hinge-shaft is hollow (for carrying instrumentation leads) and protrudes out of the CDSF windows. It is connected to drive linkages (see Fig. 3) on either side of the test section. If these linkages are anchored to the oscillating windows, a fixed leading edge droop angle (relative to the main element) results through the oscillation cycle, as in Fig. 3(c). Moving the location of the anchor point on the oscillating windows changes the magnitude of the droop angle. A continuously variable droop results if the anchor point is fixed to the tunnel sidewalls, as in Fig. 3(d). The droop value varies as $\delta_{le} = \alpha$ during the oscillation cycle.

In the variable droop mode of operation, the leading edge remains at a fixed orientation in the wind tunnel coordinate system, while the main element changes its incidence through the oscillation cycle. Following the standard convention for high-lift systems, both the angle of attack and the leading edge droop angle are defined with respect to the chordline of the main element. This design proved to be mechanically simple and very reliable for high frequency oscillations. It is important to note that application of this concept to a rotor blade requires a completely different design. Additional details of the experiment are reported in Ref. 8.

Numerical Procedure

The numerical code used for the present calculations is described in Ref. 9. This code is based on the approximate factorization implicit methodology originally developed by Beam and Warming (Ref. 10). A special feature of the code is the capability to use deformable grids. In a space fixed frame of reference the airfoil was allowed to oscillate about a prescribed mean incidence and, in addition, the deformation of the airfoil leading edge was realized. In arbitrary cases the deformation takes place within a prescribed time window of the oscillation cycle. In Ref. 11 this time window has been implemented between the mean incidence up-stroke and the mean incidence down-stroke with a maximum droop angle of 10^o at the maximum incidence of the airfoil motion. For the lower incidence part of the cycle the airfoil has its basis shape (VR12).

Different from Ref. 11, the time window in the present investigation was extended over the whole period of oscillation: the droop angle was zero at the minimum incidence and was continuously increased to a maximum droop angle corresponding to the maximum incidence of the airfoil. This special arrangement lead to a 25% leading edge flap of the airfoil which did not move whereas the rear 75% of the airfoil was rotated about the quarter chord axis according to the prescribed incidence variation. This special nose-droop device has been realized on a corresponding wind tunnel model (see Fig. 2). The numerical treatment of this case was, however, identical to the more general problem described in Ref. 11.

In order to sufficiently resolve the complex unsteady flow of an oscillating airfoil under dynamic stall conditions, a rather fine grid with 385x81 grid points was used. With this fine grid y+ of the first grid line off the airfoil surface was kept at the order of one. Of great concern was the time resolution of the calculation. In the present numerical calculations as many as 10^5 time steps per period were used with a total of 2 periods for sufficient periodic convergence. For the present calculations the Spalart-Allmaras (Ref. 12) one equation turbulence model was used. All calculations were assumed fully turbulent.

Results and Discussion

The use of both experimental measurements and numerical computations enables a more complete description of a given aerodynamic test case. These results represent a first comparison of the numerical study with measurements. Using this first level of comparison, several issues are currently under investigation including the effects of wind tunnel wall corrections in unsteady experiments and the modeling of the migration of transition during the oscillation cycle.

Computational Results

One of the key results of this study is that the general trends in measured and predicted performance agree for similar test cases, as shown in Tables 1 and 2. Both the test data and the CFD show a slight reduction in maximum lift, a large reduction in maximum drag, and a significant reduction in peak pitching moment. A direct comparison between the CFD results and the measurements is shown in Fig. 4 for two different Mach numbers of M = 0.3 and M = 0.4 at a single reduced frequency of k = 0.1. These conditions are representative of a typical retreating blade stall measured on a UH-60A BlackHawk helicopter (Ref. 13). While the lift, drag, and moment curves show qualitative agreement with the measured cases, the incremental changes between the baseline case and the variable droop case appear to be in agreement (see Fig. 4 and Tables 1 – 2). In general, the computations over predict the benefit of the VDLE for M=0.3, but more closely match the measured trends for M=0.4.

A comparison of the instantaneous pressure distributions during the cycle is shown for the M=0.3 baseline and VDLE cases in Fig. 5. For the baseline case, it appears that there is a $\Delta\alpha=2^o$ stall delay in the

computations (Figs. 5a and 5b) which may be attributed to wind tunnel wall interference effects not accounted for in the computations. However, the details of the stall, once initiated, appear to match the measurements in terms of the vortex footprint (Fig. 5b). For the VDLE case, the numerical results appear different from the measurements around the hinge line (Figs. 5c-d). There appears to be either more boundary layer thickening or mild separation aft of the hinge line observed in the measurements, but not captured in the numerical analysis. One explanation of these discrepancies may be due to the assumption of fully turbulent flow. The measured transition locations in Ref. 14 show the upstream movement of transition prior to dynamic stall. Future calculations will take into account a transition model and try to solve this problem.

Some of the key features of the variable droop results are the reduced drag and peak pitching moment that occur during the dynamic stall. As a result, the concept appears to not only improve the lift-to-drag ratio at high C_l, but also reduces the undesirable pitching moment by reducing the severity of the moment stall. One of the mechanisms for the performance gain of the VDLE is clearly shown by the CFD pressure field in Fig. 6, where the low pressure signature of the dynamic stall vortex has been reduced by the drooped leading edge. The CFD results in Fig. 7 show the Mach number distribution around the leading edge. This figure demonstrates how the VDLE concept alleviates the supersonic pocket responsible for shock boundary layer separation.

M=0.3	$\Delta C_{l\,max}$	$\Delta C_{d\,max}$	$-\Delta C_{m\,min}$
CFD	-0.22(11%)	-0.49(72%)	-0.32(68%)
EXP	-0.14(8%)	-0.35(63%)	-0.11(31%)

Table 1. Difference between baseline and VDLE performance at M = 0.3, k = 0.10

M=0.4	$\Delta C_{l\,max}$	$\Delta C_{d\,max}$	$-\Delta C_{m\,min}$
CFD	-0.20(10%)	-0.39(56%)	-0.20(43%)
EXP	-0.15(8%)	-0.36(63%)	-0.15(37%)

Table 2. Difference between baseline and VDLE performance at M = 0.4, k = 0.10

Flow Visualization

Using the technique of Point Diffraction Interferometry (Ref. 15), flow visualization images were acquired for several test cases in Fig. 8. At higher Mach numbers the mechanism for dynamic stall on the VR-12 airfoil changes from a trailing edge separation to a shock induced leading edge separation (as shown by the PDI images in Fig. 8). As a result, since the successful application of active stall control to a rotor requires a technique that works over a range of Mach numbers, two different stall mechanisms must be addressed.

Measured Results for M = 0.3 k = 0.10

The measured pressure contours during the upstroke for the M = 0.30 , k = 0.10 case are shown in Fig. 9 for the baseline (zero droop) configuration and in Fig. 10 for the variable droop configuration. For the baseline case, Fig. 9 has a peak suction pressure reaching just beyond the critical value. As a result, severe adverse pressure gradients form near the airfoil leading edge. Just after the angle of attack where the magnitude of the adverse pressure gradient reaches a maximum, a stagnation region of separated flow occurs near the trailing edge and moves forward. This subtle flow feature of trailing edge separation is then accompanied by the formation of a dynamic stall vortex near 30% chord. The presence of the vortex is marked in Fig. 9 by the low pressure ridge moving downstream with increasing angle of attack.

With the formation and convection of the vortex along the airfoil chord, the suction peak collapses in two phases. During the formation of the vortex, the peak collapses rapidly to approximately half of its final value. Following this first phase, the vortex convection is then marked by a gradual roll-off of the suction peak to its final value at the top of the upstroke. This sequence of events (initiated by trailing edge separation and followed by the formation and convection of the vortex) creates the double peak in the lift coefficient shown in Fig. 11 prior to the stall angle.

In comparison, Fig. 10 indicates that variable droop alleviates the severe adverse pressure gradients associated with the build-up of a large leading edge suction peak. A mild trace of a weak stall vortex still appears; however, the collapse of the leading edge suction peak observed in Fig. 9 does not occur with the variable droop case in Fig. 10.

The associated lift, drag, and pitching moment curves are shown in Figs. 11-13 for zero droop, fixed droop, and variable droop. Also shown, are the results for a quasi-static case with zero droop at low reduced frequency on the order of $k \approx 0.002$. In terms of the lift behavior, the fixed droop case increases the zero lift angle but maintains the same lift curve slope (as expected based on thin airfoil theory). The fixed droop softens the stall and removes the double peak found in the baseline lift curve; however, the maximum lift coefficient is slightly reduced. This can be attributed to weakening the dynamic stall vortex and therefore the induced lift. The lift behavior of the variable droop case follows the baseline at low angle of attack and then transitions to the fixed droop case near 10 deg angle of

attack. This is the angle where the variable droop is equal to the fixed droop of 10 deg. As a result, the zero lift angle is not changed significantly, but the lift curve slope is reduced. At the high angles, the variable droop reaches δ_{le}=20 deg, and stall is alleviated, but again the drooped leading edge causes a reduction in the maximum lift coefficient. Another possible source for the reduced Cl_{max} could be the influence of the hinge line on the boundary layer; however, the numerical results predicted the same reduction while assuming a smooth transition with no hinge line in the computational grid.

In terms of the drag curves in Fig. 12, the fixed droop reduces the peak drag to near the baseline quasi-static value. The drag is reduced over the high angle of attack range for both the fixed and variable droop cases. An important result is that the variable droop case reduces the peak pressure drag levels by a factor of nearly three (as predicted by the numerical results). At low angles of attack, the drag penalty of the fixed droop case increases the α=0 drag by a factor of three (see Fig. 12). This is the same penalty found for slotted airfoils applied to rotor blades (Ref. 3).

Another advantage of the variable droop concept is the reduction of the peak pitching moment during stall shown in Fig. 13. While the fixed droop case shows a slight reduction, the variable droop case restores the peak moment coefficient to near the quasi-static value. In addition, there is a large pitching moment penalty at low angles of attack caused by the fixed droop case (see Fig. 13). The large drag and moment penalties associated with fixed droop at low angles (Figs. 12-13) illustrate the need for a variable droop instead of fixed droop. Clearly, fixed droop would cause a large performance penalty on the advancing side of the rotor disk.

A key result that was not completely predicted by the numerical analysis is shown in Fig. 14. The negative pitch damping that occurs in the baseline moment curve was completely eliminated by the variable droop. The CFD results show a slight reduction in the amount of negative damping, but a cross-over still occurs in Fig. 4. It is interesting to note this result was predicted by earlier numerical computations using the ZETA code in support of water tunnel testing of the same VDLE concept (Ref. 5) applied to a VR-12. As a result, this concept shows promise with regard to preventing common rotor blade aeroelastic instabilities associated with pitch damping. In addition, the large reduction in drag may also reduce the severity of lead-lag instabilities that are excited by the impulsive drag force attributed to severe dynamic stall. One recommendation from this study is that the VDLE airfoil measurements be used in a comprehensive analysis to study some of these aeroelastic stability issues in more detail.

Measured Results for M = 0.4 k = 0.10

As shown by the flow visualization images in Figs. 8f and 8g, the change in Mach number from M=0.3 to M=0.4 alters the mechanism causing boundary layer separation. The VR-12 airfoil switches from a trailing edge stall to a leading-edge, shock-induced stall. A successful flow control technique must be able to cope with both trailing edge and leading edge separation. For the M=0.4 case, the footprint of the shock (visible in Fig. 8f) appears in the pressure distribution of Fig. 15 prior to the formation of the stall vortex. This additional flow feature is not observed in the M=0.3 pressure distribution in Fig. 9. The result of using the VDLE concept prevents the formation of a supersonic pocket near the leading edge, and so no shock boundary layer interaction occurs in Fig. 16. The signature of the stall vortex is greatly reduced, and there is only a slight roll-off of the peak suction pressure.

The corresponding forces and moments for the M=0.4 case are shown in Figs. 17-19. In contrast to the M=0.3 case, the VDLE maximum lift is greater than the fixed droop in Fig. 17. Another difference is that the peak drag coefficient is only slightly reduced for the VDLE compared to fixed droop in Fig. 18. Both the fixed and variable droop cases show a large reduction in the peak drag, as was observed for the M=0.3 case (Fig. 12). The major difference between the M=0.3 and M=0.4 results is that the 10° fixed droop reduced the magnitude of the peak pitching moment more than the VDLE in Fig. 19. This indicates that the full 20° droop range of the VDLE may be excessive for the higher Mach number case. The VDLE does, however, eliminate the negative torsional damping that is only slightly changed by the fixed droop. As in the M=0.3 case, the low angle of attack drag and moment penalties are observed for the fixed droop.

Application to Rotor Stall Alleviation

According to Ref. 16, it is the ratio of the maximum lift to both the minimum pitching moment and the maximum drag that determines the relative merit of a rotor stall alleviation concept. Using a dynamic stall function for both the pitching moment and the drag (as in Ref. 16), the relative merits of the VDLE airfoil are summarized in Fig. 20. The measurements shown in this figure cover a range of reduced frequency and Mach number representative of moderate retreating blade stall (Ref. 13). As shown by Fig. 20, the general trend of the VDLE is to reduce the magnitude of the peak drag and pitching moment while only slightly reducing the maximum lift coefficient.

Future work on application of this concept to a rotor includes the identification of optimum droop schedules, chordwise hinge location, and radial location

of the drooping section. The mechanical design and integration of a variable droop leading edge airfoil into a full-scale rotor blade remains a challenge, however these results provide motivation for further research and development of this concept.

Conclusions

(1) An effective compressible dynamic stall control technique using the VDLE airfoil has been presented in this paper. Both flow visualization and unsteady pressure measurements over a VDLE airfoil were obtained for a wide range of flow conditions and airfoil configurations. These include the baseline no-droop airfoil, the fixed-droop airfoil, and the VDLE airfoil.
(2) Preliminary results clearly demonstrate the ability of the VDLE airfoil to control the dynamic stall process for different stall onset mechanisms, while avoiding the low angle of attack penalties associated with other high-lift systems. Significant decreases in the peak drag and pitching moment coefficients were found in both the measurements and CFD, thus validating this flow control concept.
(3) The measured results showed an additional benefit where the negative torsional damping caused by dynamic stall was completely eliminated by the variable droop leading edge concept.
(4) For the baseline case, it appears there is a $\Delta\alpha=2^{o}$ stall delay in the computations at M=0.3, and a slight difference in the flow over the hinge line. While the computed lift, drag, and moment curves show qualitative agreement with the measured cases, the incremental changes between the baseline case and the variable droop case appear to be in quantitative agreement.

Acknowledgments

This work was performed under the US Army / Germany Memorandum of Understanding (MOU) with K. McAlister and W. Geissler as the principal investigators. The numerical work was performed by DLR and the experiments were conducted by the US Army. The VDLE concept was developed by Chee Tung. Larry Carr and Mike Wilder initiated work on the wind tunnel model design and data acquisition system.

References

[1] Chandrasekhara, M.S., Wilder, M.C., and Carr, L. W., "Compressible Dynamic Stall Control Using Dynamic Shape Adaptation," AIAA Paper 99-0655, 1999.
[2] Carr, L.W., Chandrasekhara, M.S., Wilder, M.C., and Noonan, K.W., "Effect of Compressibility on Suppression of Dynamic Stall Using a Slotted Airfoil," (AIAA Paper 98-0332), *Journal of Aircraft*, Vol. 38, No. 2, pp.296-309, March-April. 2001.
[3] Yeo, H., and Lim, J. W., "Application of a Slotted Airfoil for UH-60A Helicopter Performance," AHS: Aerodynamics, Acoustics and Test and Evaluation Technical Specialist Meeting, San Francisco, CA, January 23-25, 2002.
[4] Yu, Y.H., Lee, S., McAlister, K.W., Tung, C. , and Wang, C.M., "Dynamic Stall Control for Advanced Rotorcraft Application," *AIAA Journal*, Vol. 33, No. 2, pp. 289-295.
[5] Lee, S., McAlister, K., and Tung, C., "Characteristics of Deformable Leading Edge for High Performance Rotor," AIAA 11th Applied Aerodynamics Conference, August 9-11, Monterey CA, 1993.
[6] Chandrasekhara, M.S., Wilder, M.C., and Carr, L. W., "On the Competing Mechanisms of Compressible Dynamic Stall," (AIAA Paper 96-1953), *AIAA Journal*, Vol. 36, No. 3, March 1998, pp. 387-393.
[7] Carr, L.W., and Chandrasekhara, M.S., "Design and Development of a Compressible Dynamic Stall Facility," *Journal of Aircraft*, Vol. 29, No. 3, May-June 1992, pp. 314-318.
[8] M.S.Chandrasekhara, Martin, P.B., Tung, C., "Compressible Dynamic Stall Using a Variable Droop Leading Edge Airfoil," (AIAA Paper 2003-0048), 2003.
[9] Geissler, W. "Verfahren in der Instationären Aerodynamik (Methods in Unsteady Aerodynamics) ," DLR-FB 93-21 , 1993.
[10] Beam,R., and Warming,R.F., "An Implicit Factored Scheme for the Compressible Navier-Stokes Equations," AIAA J. Vol.16, No.4 (April 1978).
[11] Geissler, W., and Trenker,M., "Numerical Investigation of Dynamic Stall Control by a Nose-Droop Device," AHS: Aerodynamics, Acoustics and Test and Evaluation Technical Specialist Meeting, San Francisco, CA, January 23-25, 2002.
[12] Spalart, P., and Allmaras, S.R., "A One Equation Turbulence Model for Aerodynamic Flows," AIAA-paper 92-0439, January 1992.
[13] Bousman, W. G., "Airfoil Design and Rotorcraft Performance," American Helicopter Society, 58th Annual Forum, Montreal Canada, June 11-13, 2002.
[14] Chandrasekhara, M. S., and Wilder, M. C., "Heat Flux Gage Studies of Compressible Dynamic Stall," (AIAA Paper 2002-0291) to appear in *AIAA Journal*.
[15] N.Brock, M.S.Chandrasekhara, and L.W.Carr, "A Real Time Interferometry System for Unsteady Flow Measurements," ICIASF'91 RECORD, IEEE Publication 91CH3028-8, pp. 423-430.
[16] Bousman, W. G. , "Evaluation of Airfoil Dynamic Stall Characteristics for Maneuverability," 26th European Rotorcraft Forum, The Hague, Netherlands, Sept. 26-29, 2000.

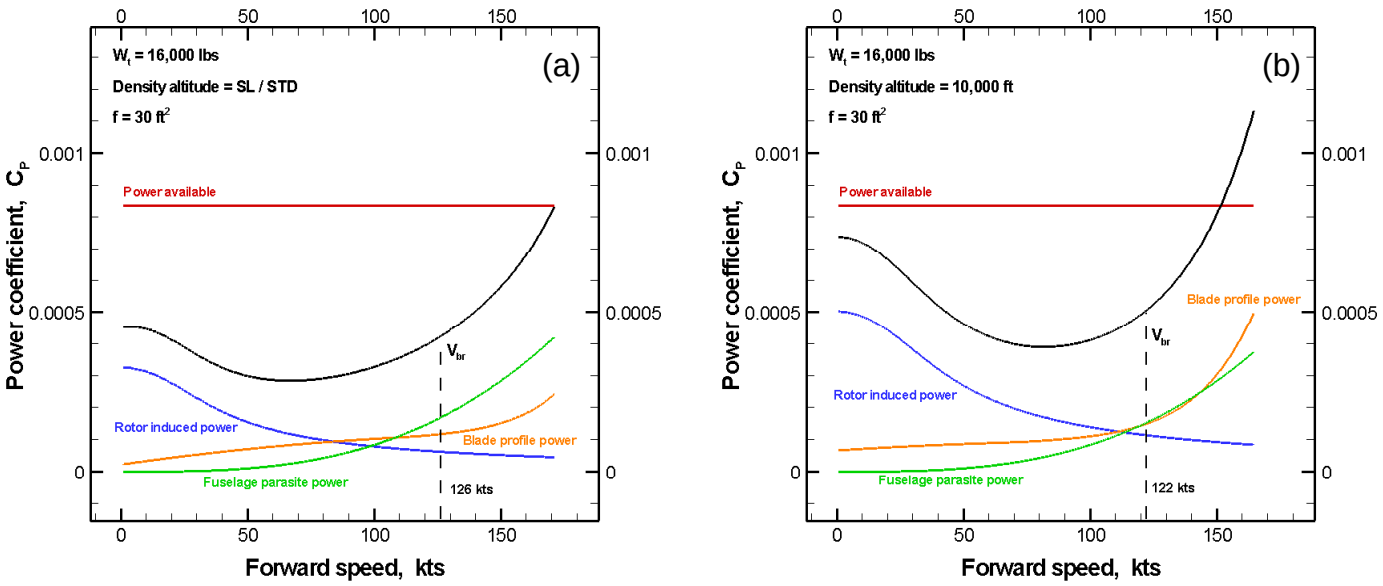

Fig. 1. Power breakdown estimate at (a) sea level and at (b) 10,000ft density altitude.

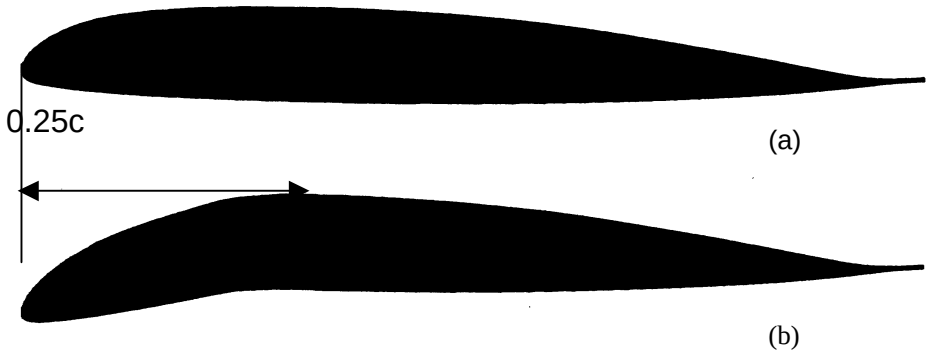

Fig. 2. Baseline VR-12 airfoil (a) baseline airfoil (b) drooped leading edge.

(a)

(b)

(c)

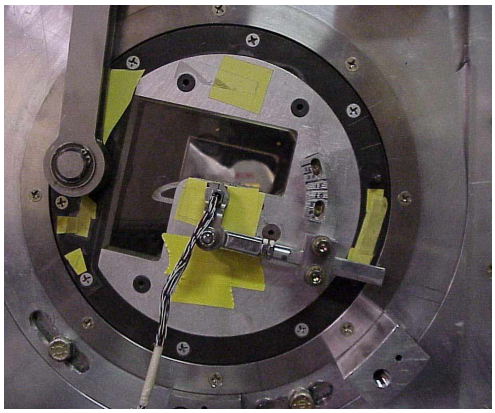

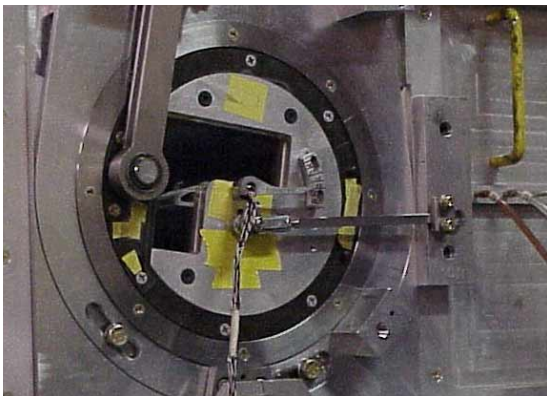

(d)

Fig. 3. VDLE airfoil and wind tunnel mounting configurations.

(a) VDLE airfoil model with leading edge detached
(b) VDLE airfoil with leading edge assembled
(c) Leading edge cam mounted to rotating frame of reference for fixed droop
(d) Leading edge cam mounted to fixed frame of reference for variable droop

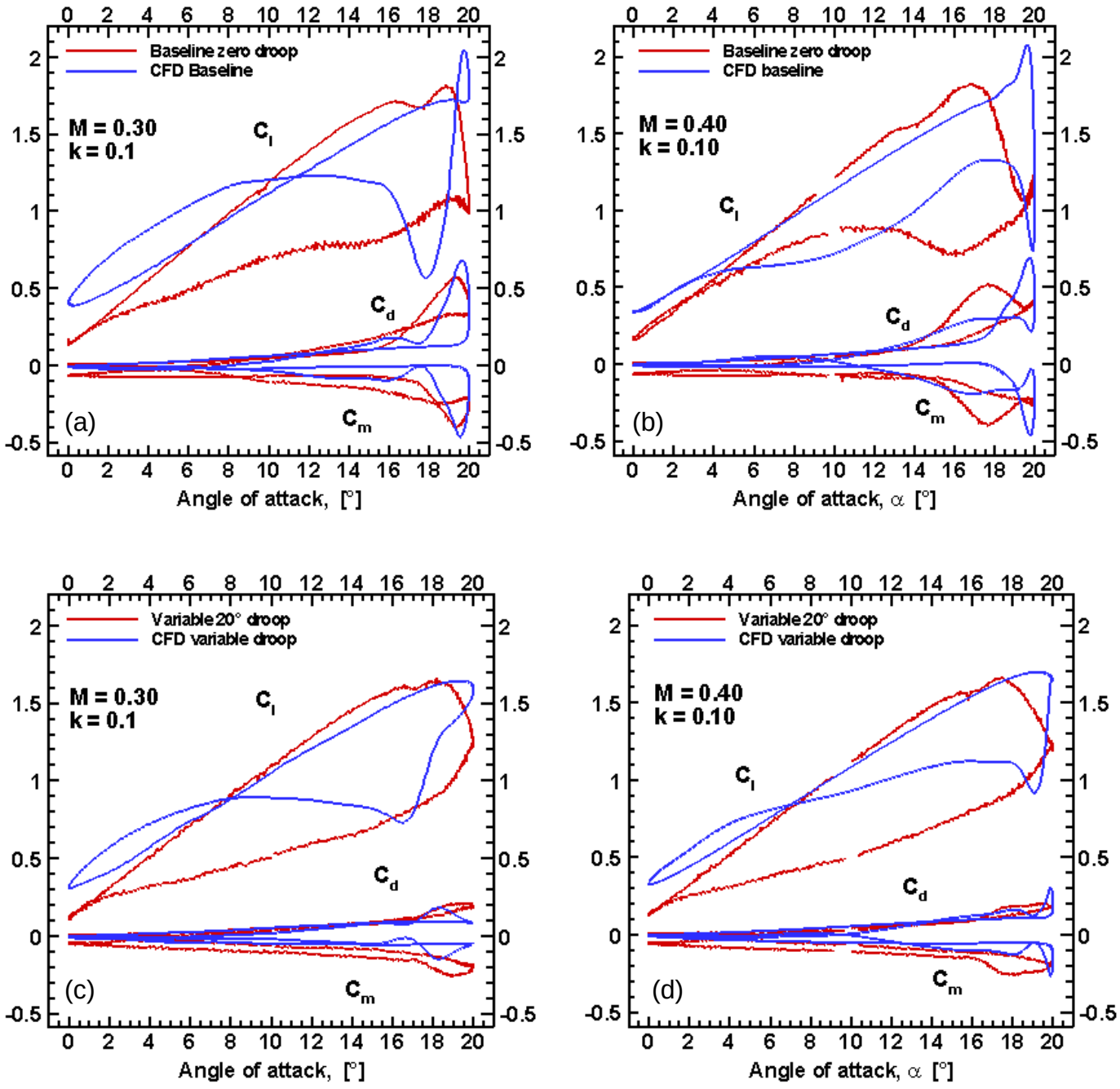

Fig. 4: CFD results compared to measurements.

(a) M = 0.3 , k = 0.10 baseline droop
(b) M = 0.4 , k = 0.10 baseline droop
(c) M = 0.3 , k = 0.10 variable droop
(d) M = 0.4 , k = 0.10 variable droop

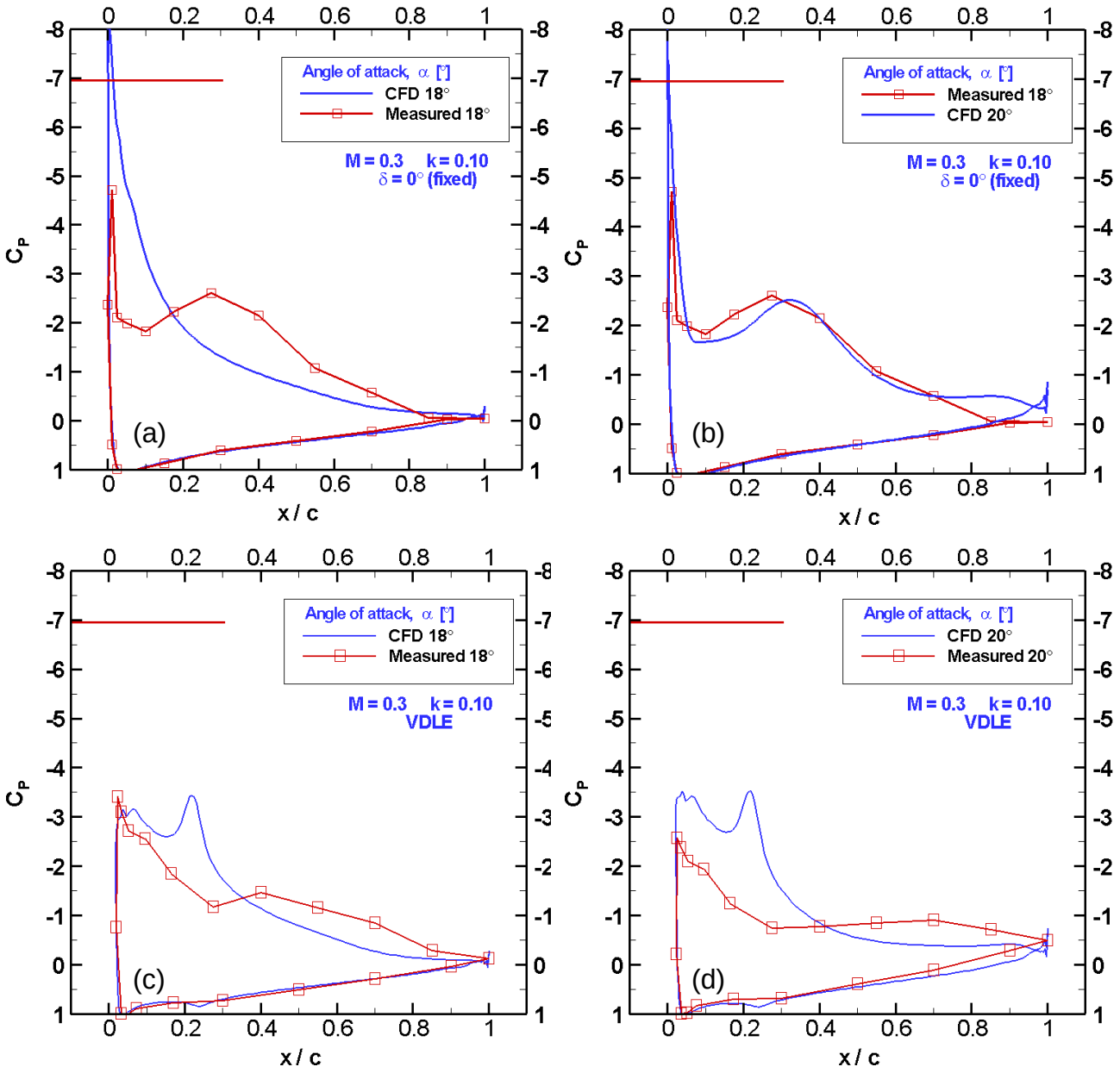

Fig. 5: Pressure comparisons for M=0.3 , k = 0.10 during the upstroke.

(a) Baseline CFD compared to measurements at α=18°
(b) Baseline CFD at α=20° compared to measurements at α=18°
(c) VDLE CFD compared to measurements at α=18°
(d) VDLE CFD compared to measurements at α=20°

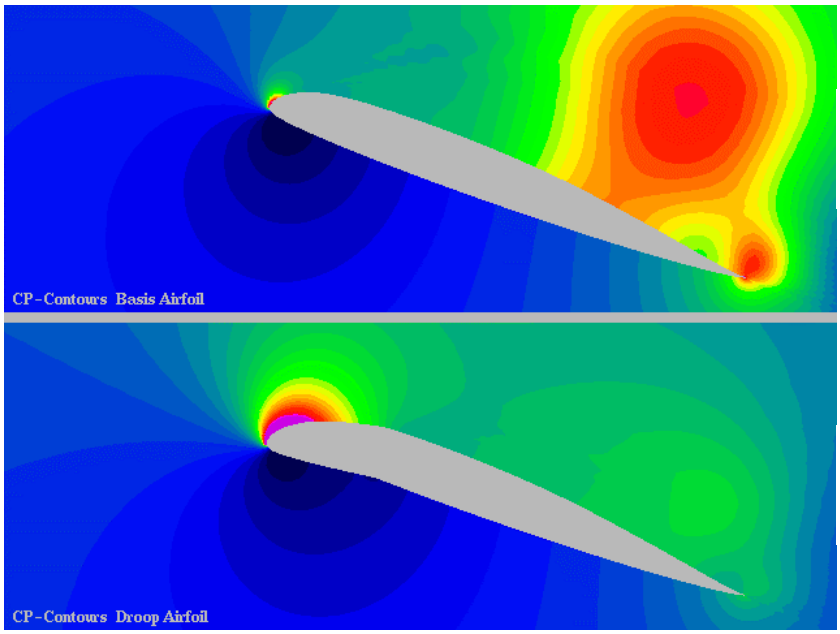

Fig. 6: CFD Pressure contours at 19.7° (upstroke).

(a) baseline (no droop)
(b) variable droop leading edge

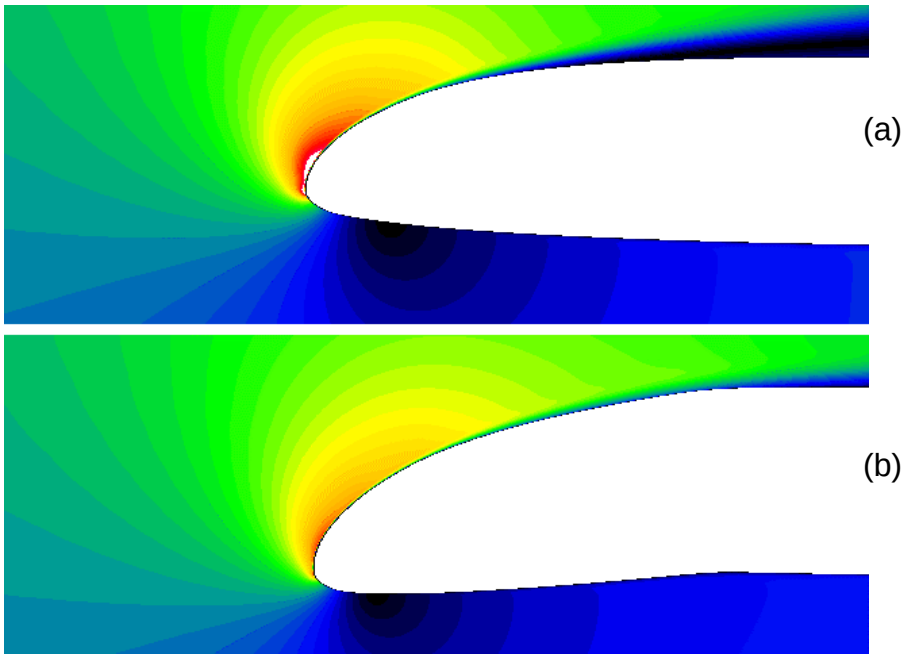

Fig. 7: CFD Mach contours at 18.4° during upstroke.

(a) baseline (no droop)

(b) variable droop leading edge

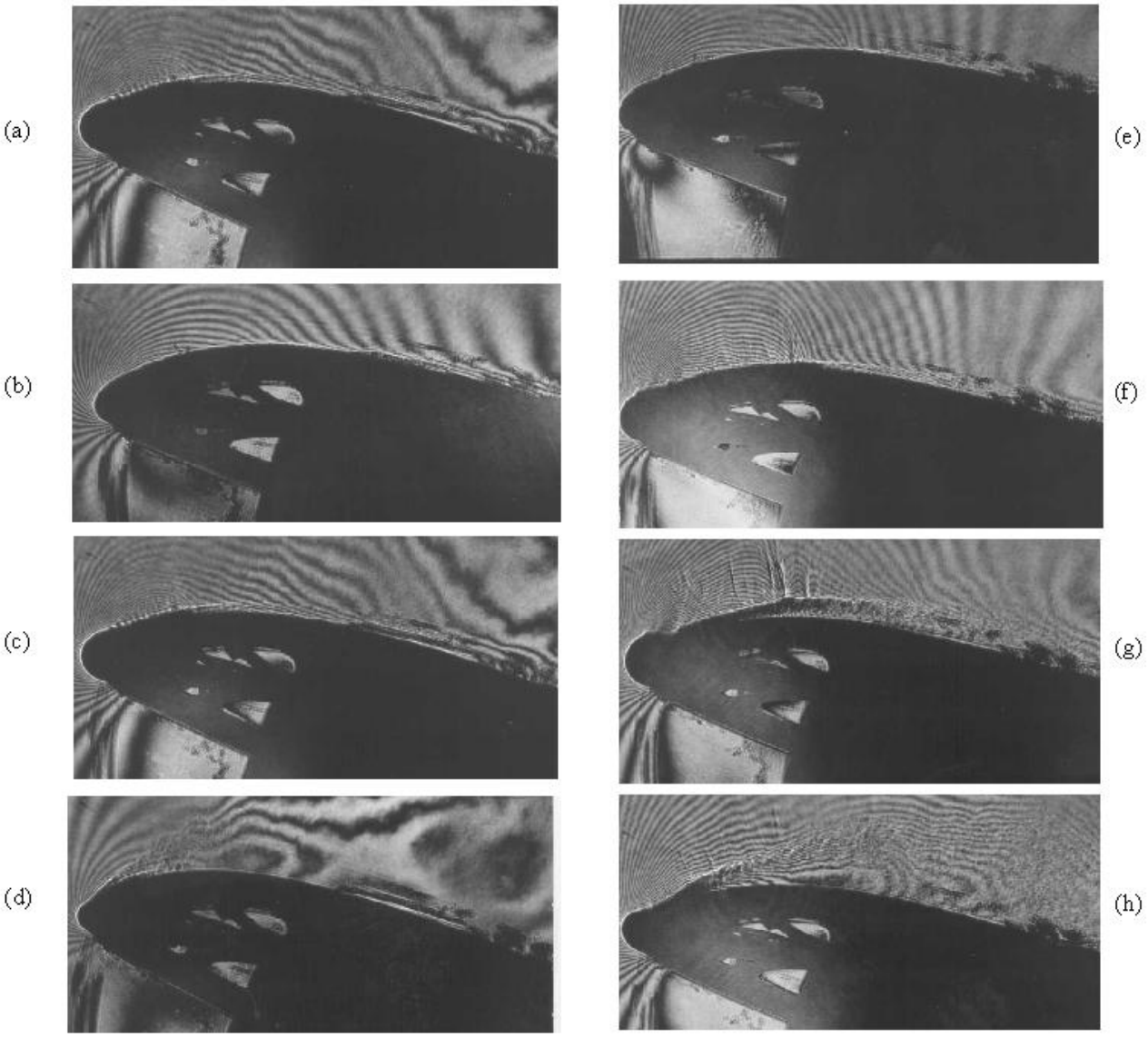

Fig. 8: Point Diffraction Interferometry images of baseline VR-12 dynamic stall during the upstroke.

(a) M = 0.3, k = 0.10, α=12.5 deg
(b) M = 0.3, k = 0.10, α=17.0 deg
(c) M = 0.3, k = 0.10, α=18.0 deg
(d) M = 0.3, k = 0.10, α=20.0 deg
(e) M = 0.4, k = 0.10, α= 9.8 deg
(f) M = 0.4, k = 0.10, α=12.5 deg
(g) M = 0.4, k = 0.10, α=14.0 deg
(h) M = 0.3, k = 0.10, α=15.0 deg

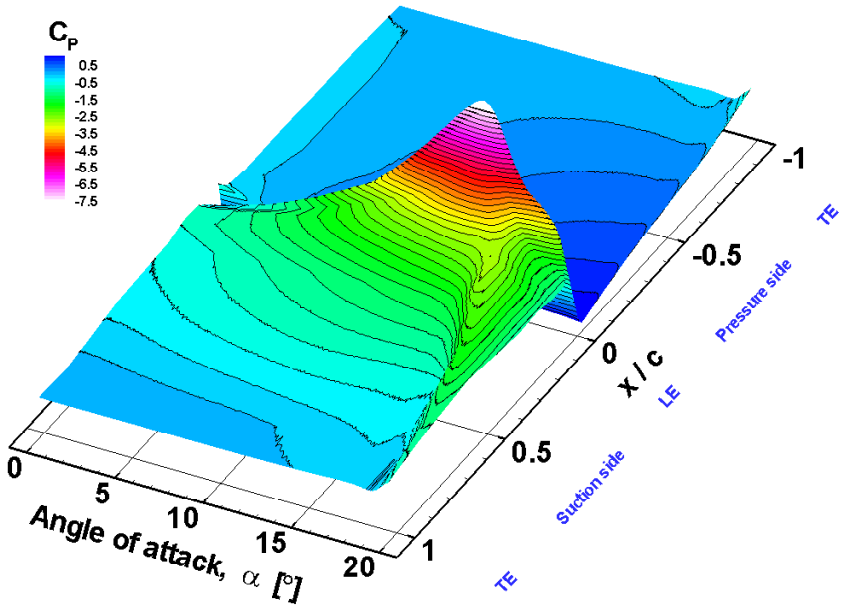

Fig. 9: Pressure contours during the upstroke

M = 0.3 , k = 0.10 , zero droop baseline.

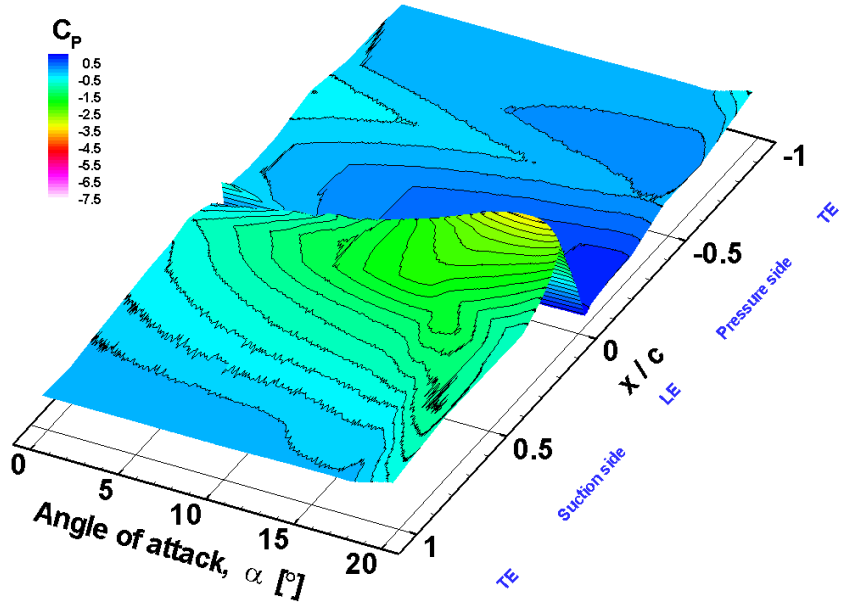

Fig. 10: Pressure contours during the upstroke

M = 0.3 , k = 0.10 , variable droop case.

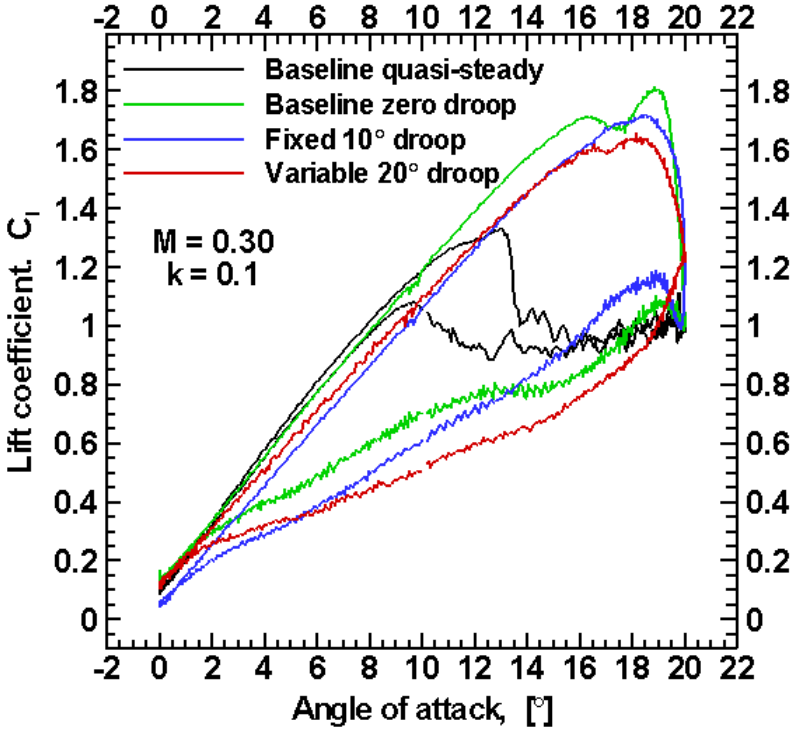

Fig. 11: Lift coefficient integrated from measured pressure distributions.

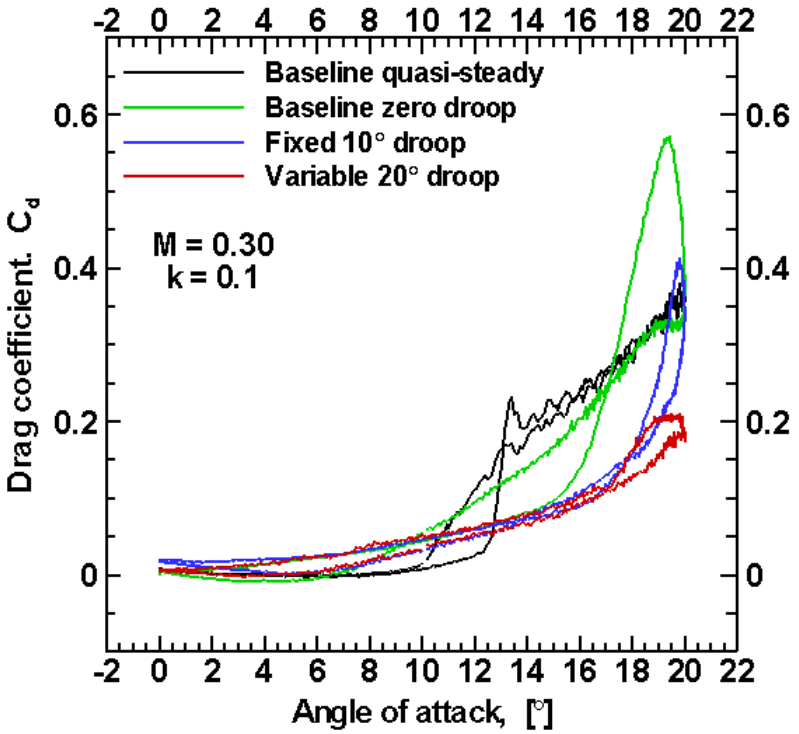

Fig. 12: Drag coefficient integrated from measured pressure distributions.

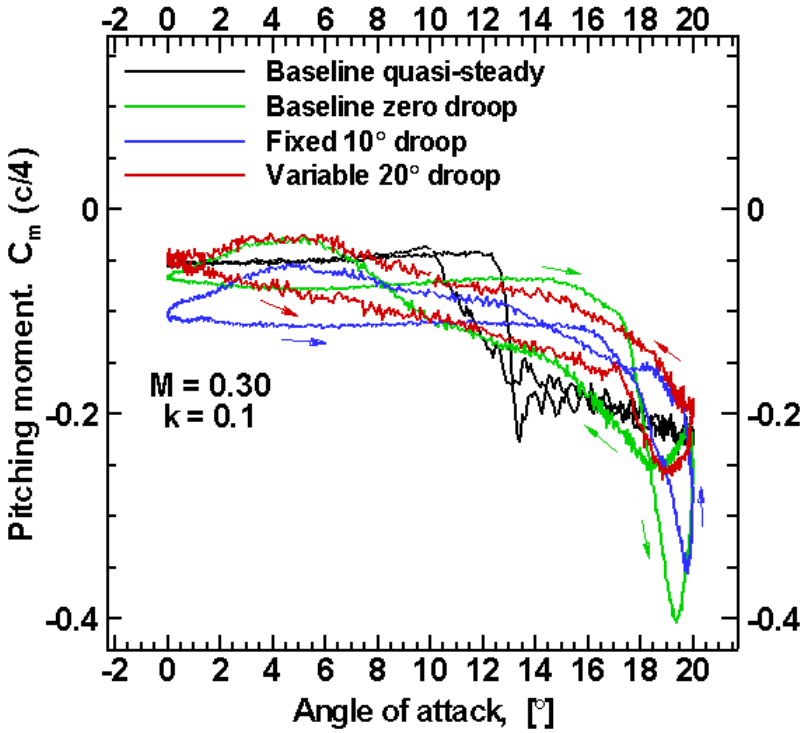

Fig. 13: Moment coefficient integrated from measured pressure distributions.

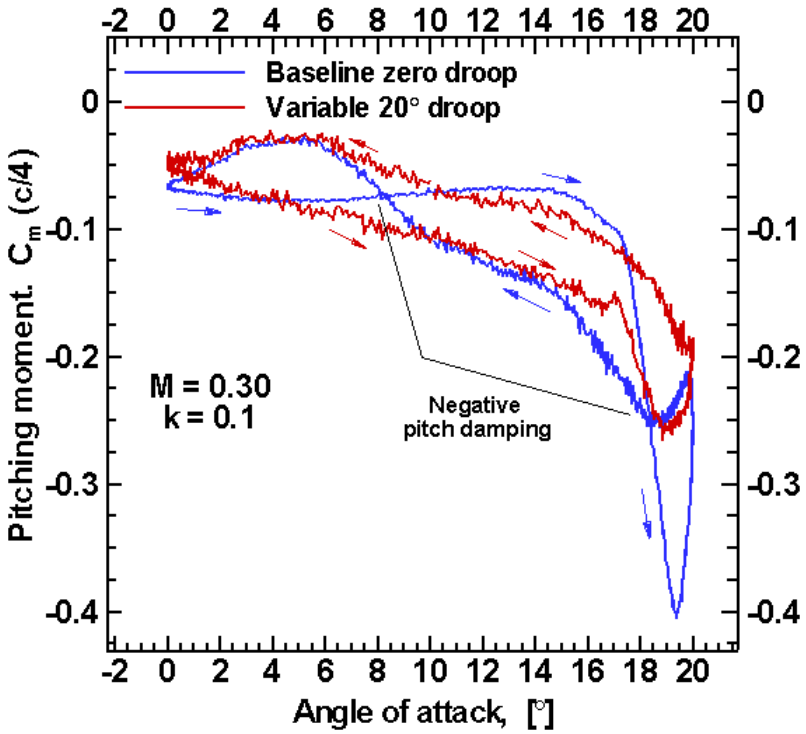

Fig. 14: Elimination of negative pitch damping.

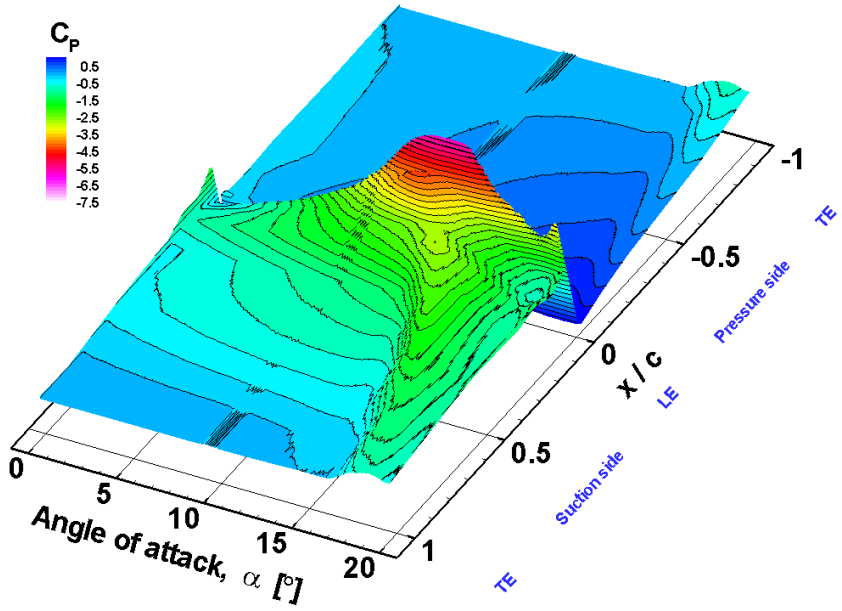

Fig. 15: Pressure contours during the upstroke

M = 0.4 , k = 0.10 , zero droop baseline.

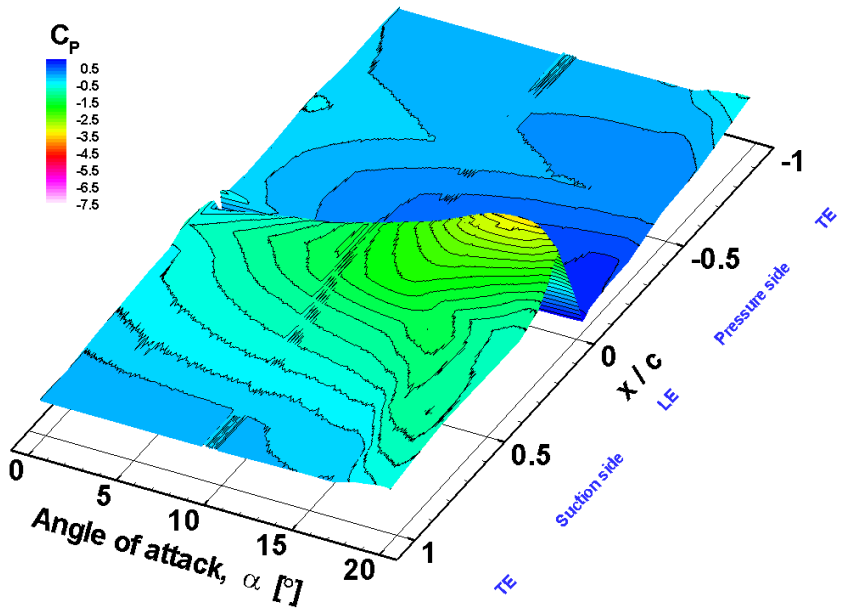

Fig. 16: Pressure contours during the upstroke

M = 0.4 , k = 0.10 , variable droop case.

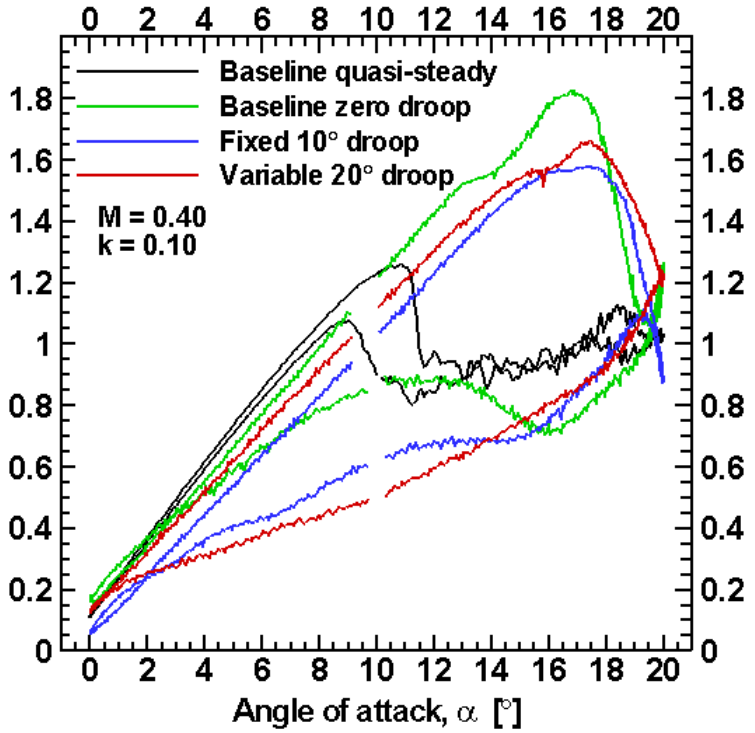

Fig. 17: Lift coefficient integrated from measured pressure distributions.

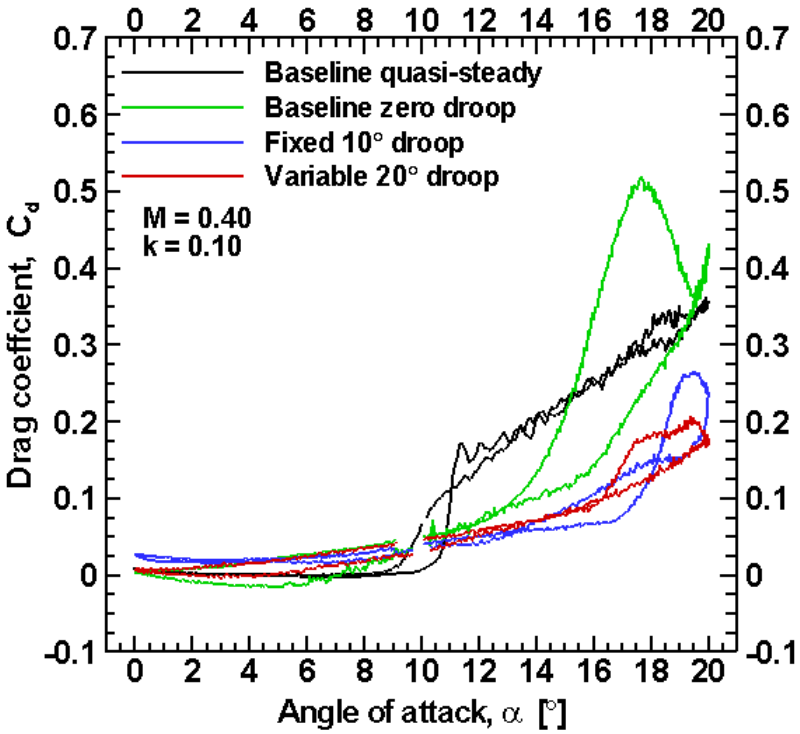

Fig. 18: Drag coefficient integrated from measured pressure distributions.

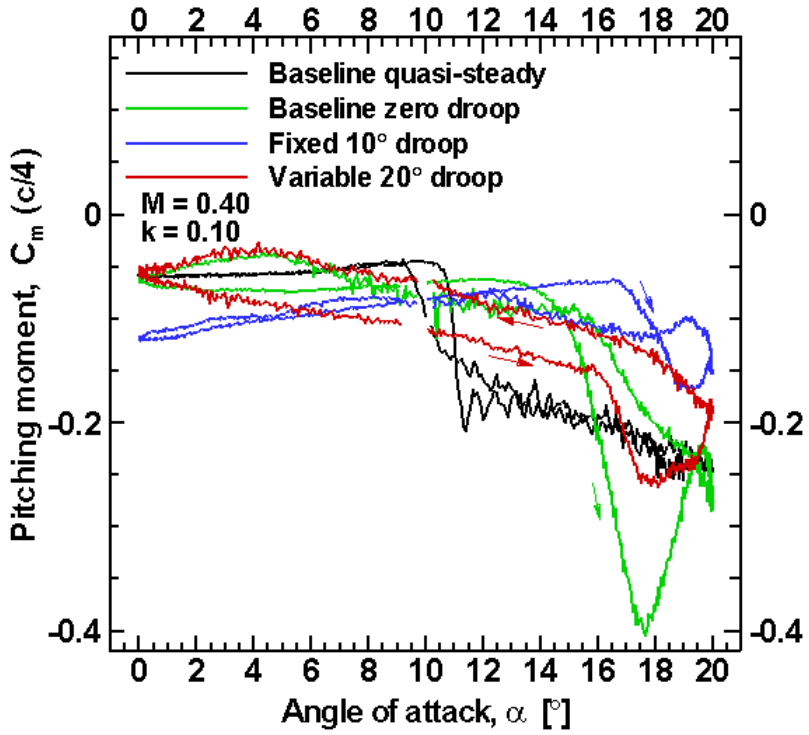

Fig. 19: Moment coefficient integrated from measured pressure distributions.

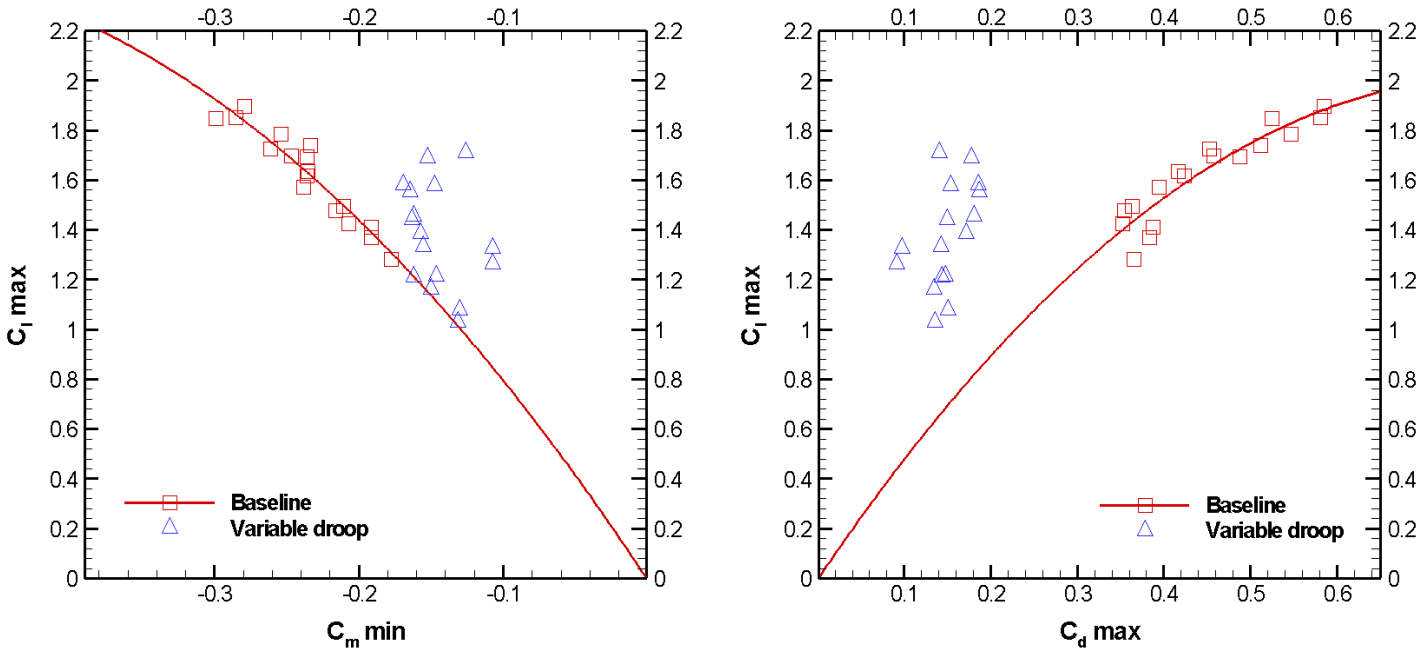

Fig. 20: Bousman's dynamic stall function (Ref. 15) for the VR-12 with and without variable droop (mean angle 10 deg , k=0 to 0.1 , and M = 0.2 to 0.4).